Air-sea interaction over the eastern Pacific warm pool: Gap winds, thermocline dome, and atmospheric convection

Shang-Ping Xie*

International Pacific Research Center and Department of Meteorology

University of Hawaii, Honolulu, Hawaii

Haiming Xu

International Pacific Research Center, University of Hawaii, Honolulu, Hawaii

William S. Kessler

Pacific Marine Environmental Laboratory, NOAA, Seattle, Washington

Masami Nonaka

Frontier Research System for Global Change, Yokohama, Japan

Journal of Climate

March 22, 2004, submitted

* Corresponding author address: Shang-Ping Xie, International Pacific Research Center, SOEST, University of Hawaii, Honolulu, HI 96822.

E-mail: xie@hawaii.edu

ABSTRACT

High-resolution satellite observations are used to investigate air-sea interaction over the eastern Pacific warm pool. In winter, strong wind jets develop over the Gulfs of Tehuantepec, Papagayo and Panama, accelerated by the pressure gradients between the Atlantic and Pacific across narrow passes of Central American cordillera. Patches of cold sea surface temperatures (SSTs) and high chlorophyll develop under these wind jets as a result of increased turbulent heat flux from the ocean and enhanced mixing across the bottom of the ocean mixed layer. Despite a large decrease in SST that exceeds 3^{o}C in seasonal means, the cold patches associated with the Tehuantepec and Papagayo jets do not have an obvious effect on local atmospheric convection in winter since the intertropical convergence zone (ITCZ) is located further south. The cold patch of the Panama jet to the south, on the other hand, cuts through the winter ITCZ and breaks it into two parts.

A pronounced thermocline dome develops west of the Gulf of Papagayo, with the 20^{o}C isotherm only 30 m deep throughout the year. In summer when the Panama jet disappears and the other two wind jets weaken, SST is found to be 0.5^{o}C lower over this Costa Rica Dome than the background. This cold spot reduces local precipitation by half, punching a hole of 500 km in diameter in the summer ITCZ. The Dome underlies a patch of open-ocean high chlorophyll. This thermocline dome is an ocean dynamic response to the positive wind curls south of the Papagayo jet, which is optimally oriented to excite ocean Rossby waves that remotely affect the ocean to the west. The meridionally oriented Tehuantepec and Panama jets, by contrast, only influence the local thermocline depth with few remote effects on SST and the atmosphere. The orographical-triggered air-sea interaction described here is a good benchmark for testing high-resolution climate models now under development.

1. Introduction

The ocean-atmosphere system over the eastern tropical Pacific displays large north-south asymmetry with respect to the equator. While surface water on and south of the equator remains below 26^{o}C year around, sea surface temperature (SST) to the north off the coast of Central America is mostly above 27^{o}C, a region we hereafter refer to as the eastern Pacific warm pool. The warm pool is bounded on the south by a sharp SST front slightly north of the equator separating the equatorial cold tongue from the warm water to the north. Deep atmospheric convection with heavy precipitation is generally confined to the north of this equatorial front, with dry conditions prevailing on and south of the equator. This region of strong atmospheric convection is called the intertropical convergence zone (ITCZ), onto which the southeast and northeast trades converge. This climatic asymmetry between north and south of the equator results from air-sea interaction triggered by latitudinal asymmetries in continental geometry (see Xie 2004a for a recent review). The eastern Pacific warm pool is climatically important, supporting one of the major convection centers of the global atmosphere (Mitchell and Wallace 1992; Wang and Enfield 2003). Hurricanes that originate there travel northwestward, occasionally with devastating effects on western Mexico or southern California. Some have even reached Hawaii, 6000 km away.

The continents on the eastern boundary of the Pacific are also highly asymmetrical. The steep and high Andes separate the Pacific from much of the South American continent and the Atlantic while a mountain range runs through the narrow Central American land bridge as an extension of the Sierra Madre Occidental from North America. This Central American cordillera is about 1 km high on average, blocking airflow from the Caribbean Sea. Three major gaps penetrate this mountain range: at the isthmus of Tehuantepec, over

Lake Nicaragua, and at Panama (Fig. 1a). In boreal winter, sea level pressure is often higher over the Caribbean than on the Pacific side, forcing strong wind jets through these gaps and over the eastern Pacific warm pool. On synoptic timescales, these gap wind events may occur in sequence or independently (Chelton et al. 2000). There have been many studies on the wind jet over the Gulf of Tehuantepec during the boreal winter. Steenburgh et al.'s (1998) model simulation shows that during these high-wind events, strong pressure gradients between the Atlantic and Pacific accelerate the winds to high speeds along the narrow mountain passes. After leaving the coast, air trajectories tend to follow anticyclonic arcs, which Clarke (1988) suggests are inertial flow nearly free of pressure gradient force. In Steenburgh et al.'s (1998) model, the Atlantic air mass, with cold temperatures and high sea level pressure, penetrates a few hundred kilometers over the Gulf of Tehuantepec, and these pressure anomalies significantly modify the trajectories and cause them to deviate from the inertial circle. A cloud arc sometimes forms along the cold front and advances offshore with the cold surge over the Gulf of Tehuantepec (Schultz et al. 1997), perhaps due to the upward motion associated with gravity currents.

Figure 1a shows the January wind velocity averaged for 2000-03. The Tehuantepec jet is clearly visible in this climatological wind map, and so are two other wind jets to the south (the Papagayo and Panama jets hereafter). Wind speeds are typically 10 m/s in these climatological wind jets while winds lee of the mountain range are one order of magnitude weaker. The wind jets extend a few hundred kilometers offshore, with the Tehuantepec and Papagayo jets eventually merging into the Pacific northeast trades. The Tehuantepec and Panama jets are oriented roughly in the north-south direction while the Papagayo jet takes a more zonal orientation. As will become clear, this difference in the jet orientation results in distinct subsurface ocean response to these wind jets.

These wind jets are strongest during boreal winter, and exert a strong influence on the surface ocean as readily seen from satellite infrared observations (Clarke 1988; Legeckis 1988; Barton et al. 1993). It is quite common for SST near these wind jets to drop by a few degrees during a strong wind surge event, due to intensified surface turbulent heat flux and entrainment. Over the eastern Pacific warm pool, the thermocline is only 50 m deep or shallower. Strong wind stirring together with surface heat flux cooling is very effective in entraining cold thermocline water into the surface mixed layer. Besides the SST decreases, enhanced entrainment also gives rise to increased biological activity beneath these wind jets in winter (Fiedler 2002 and references therein).

Strong wind curl associated with the wind jets create rich structures in the thermocline over the eastern Pacific warm pool, while there is some disagreement on the importance of nonlinear ocean dynamics (Hofmann et al. 1981; McCreary et al. 1989; Umatani and Yamagata 1991; Kessler 2002). In particular, there is a thermocline dome with cyclonic circulation around it. This Costa Rica Dome is a permanent feature of the eastern tropical Pacific centered at 90^{o}W, 9^{o}N, with its position and size varying seasonally to some degree. In the Costa Rica Dome, the 20^{o}C isotherm is very close to the sea surface, only 30 m deep on long-term mean. The upwelling and mixing in this thermocline dome make it rich in nutrients, attracting marine mammals like blue whales and common dolphins (Fiedler 2002). Kessler (2002) estimates a 3.5 Sv upwelling in the Costa Rica Dome and suggests that it is an important element of the Pacific intermediate-water circulation. In particular, McCreary et al. (2002) suggest based on ocean model experiments that this upwelling drives an eastward subsurface jet north of the equator—the Tsuchiya jet—that is associated with a strong potential vorticity front in the thermocline. See Kessler (2004) for a recent review of eastern Pacific Ocean circulation.

The present study investigates the climatic effects of these Central American gap winds. These winds imprint on winter SST as cold patches over the otherwise warm water from 5-15^{o}N. Kessler (2002) further notes an "isolated cool spot near 9^{o}N, 90^{o}W" (e.g., Fig. 4) in annual-mean SST that "marks the surface expression of the Costa Rica Dome." It is unclear, however, whether this cold spot results exclusively from gap wind's effect in winter or such an SST expression of the Dome is seen in other seasons as well. While there are several studies of the gap wind effect on ocean, to our knowledge, the feedback of gap wind-induced SST changes on the atmosphere has not been discussed in the literature. Given high background SSTs over the eastern Pacific warm pool that exceed the convective threshold (~27^{o}C), cold spots induced by gap winds would conceivably suppress local convection. The coarse spatial resolution of rainfall estimates based on space-borne infrared remote sensing may have hindered this SST feedback from being detected. For example, the widely used CMAP product (Xie and Arkin 1996) has a resolution of 2.5^o, the same scale as the cold spots in the eastern Pacific warm pool.

The present study takes advantage of recent observations by space-borne microwave instruments and examines the gap wind-induced air-sea interaction over the eastern Pacific warm pool, including the ocean-to-atmospheric feedback. These microwave observations allow a more direct inference of rainfall and at higher resolution than infrared sensing, and measure SST nearly free of clouds. Unlike many previous studies on synoptic wind events, our focus is on monthly and seasonal timescales. Specific questions we would like to address are: How do these winds force variations in SST and the subsurface ocean? Does the shallow thermocline of the Costa Rica Dome have a significant effect on SST? Do these SST signatures of gap winds influence atmospheric convection and does this influence vary with season? The first question has been addressed to some degree in previous studies, but new satellite observations of the ocean and atmosphere now allow us to synthesize various aspects and gain a physically consistent picture of this air-sea interaction. Our analysis shows that in boreal summer when the gap winds are weak, the Costa Rica Dome maintains a cold spot, which in turn suppresses local atmospheric convection. Somewhat surprisingly, the ocean-to-atmospheric feedback is less clear in boreal winter despite strong gap winds.

The rest of the paper is organized as follows. Section 2 describes the datasets. Section 3 presents the results, and Section 4 is a summary.

2. Data

This study analyzes a suite of satellite observations of SST, sea surface height (SSH), sea surface wind, and chlorophyll by several different sensors on different platforms. These new satellite observations offer a view of the oceans and the overlying atmosphere in detail never possible before, stimulating a recent flurry of air-sea interaction studies (see Xie 2004b for a recent review, and references therein).

The Tropical Rain Measuring Mission (TRMM) satellite's microwave imager (TMI) measures SST nearly free of cloud influence over the global tropics within 38ºN/S, at resolutions of 0.25º in space and 2~3 days in time. This microwave remote sensing substantially improves the sampling of SST over cloudy regions like the eastern Pacific warm pool. TMI also measures rain rate at the same resolution. We use a monthly TMI product available from January 1998 to December 2003 on a 0.25º grid (Wentz et al. 2000). There are considerable uncertainties in quantitative rainfall estimates using satellite observations. Here we limit ourselves to a qualitative discussion of spatial variations in rainfall in response to gap winds and solar seasonal cycle. We will compare this TMI product with other independent measurements of rainfall onboard TRMM. On a 0.5º grid, the 3A25G2 product is based on the precipitation radar (PR) observations. PR makes the best estimate of precipitation but its narrow swath introduces larger sampling errors for climatological averages. On a 1º grid, the 3B43 product combines infrared observations by TRMM and geostationary satellites and rain gauges, which is an indirect inference of rainfall over the ocean but enjoys good sampling and coverage. The PR and infrared products provide rainfall over both land and ocean while the TMI product is limited to the open ocean.

The microwave scatterometer on the QuikSCAT satellite measures daily surface wind velocity over the world ocean (Liu et al. 2000). QuikSCAT observations have revealed rich wind structures on short spatial scales around the world (Chelton et al. 2004). We use a monthly product for wind velocity for August 1999-December 2003 on a 0.25º grid.

The Sea-viewing Wide Field-of-view Sensor (SeaWiFS) satellite measures ocean color and chlorophyll concentration from October 1997 to November 2003, which are often a good indicator of ocean upwelling. We use monthly averages on a 0.25º grid.

The upper thermocline depth, when shallow, can have important effects on SST. We use the 20ºC isotherm depth based on a monthly ocean temperature climatology on a 1º x 1º grid, which is derived from historical expendable bathythermograph (XBT) observations.

Most temperature profiles were during 1979 through 1992, and a smaller number of profiles after that date are also used in constructing the climatology. This XBT climatology compares quite well with independent SST observations. See Kessler (2002) for a detailed description of this dataset.

Altimeters on the European Remote Sensing (ERS) and TOPEX/Poseidon (T/P) satellites measure SSH deviations from its long-term mean at their nadir. There is a tradeoff between spatial and temporal resolution: T/P has a 10-day repeat orbit with a wide zonal spacing between ground-tracks, while ERS has a 35-day repeat orbit with a small track spacing. We use a merged SSH dataset that takes advantage of both T/P's high temporal and ERS's high spatial resolutions (Ducet et al. 2000), available from October 1992 to July 2001 on a 0.25º grid. We use this merged SSH dataset to infer the seasonal cycle in thermocline depth.

Monthly climatologies are constructed for TRMM SST and rainfall, QuikSCAT surface wind velocity, merged ERS-T/P SSH, and SeaWiFS chlorophyll for periods these observations are available. The discussion that follows is limited to these multi-year climatologies, while sub-monthly and interannual variability is beyond the scope of this study. See Wang et al. (2003) and Chiang (2000) for recent studies of interannual variability over the region and its effect on the Atlantic. In general, signals to be discussed here are well above measurements errors. We refer to relevant references in the above for satellite-data error analysis. For our analysis, we use several independent measurements, which turn out to yield mutually corroborating and physical consistent results. Such physical consistency gives us confidence in the results.

3. Results

a. Wind jets

In the paper, we discuss the Central American wind jets based on the monthly mean climatology, although there is considerable variability on the synoptic timescales (Chelton et al. 2000). Our use of monthly climatology is based on the linear assumption that the low-frequency forcing drives the low-frequency ocean circulation (Kessler 2004). During winter, all the three jets are well developed on the Pacific side of the major mountain passes (Fig. 1). By contrast, winds are generally low in the lee of the Central American mountains with elevations above 1 km.

While previous studies have focused exclusively on the winter jets, Figure 1 shows the full seasonal cycle of these wind jets along the longitude or latitude where their axes leave the coast. The Tehuantepec jet is strongest during October-February, but a weaker northerly wind jet remains visible in summer over the Gulf of Tehuantepec. The Papagayo and Panama jets display slightly different seasonality, peaking in December-April. While the Panama jet ceases to occur after April, the Tehuantepec and Papagayo jets persist in other months with reduced speeds. The Papagayo jet disappears altogether only in September, the time the Tehuantepec jet is also at its minimum. Both the Tehuantepec and Papagayo jets show a secondary peak during July-August, for reasons that are not clear at this time.

In the following, we will display several figures in a common format for easy comparison among various observations. Each figure has three panels for annual, January-April and July-October means, respectively. January-April are months when the ITCZ is close to the equator (Fig. 2) and all the three wind jets are all reasonably strong. The ITCZ moves to its northernmost latitudes during July-October.

Figure 3 shows the wind stress vectors and Ekman pumping velocity, $w_e = curl(\boldsymbol{\tau} / f\rho)$, where τ is the wind stress vector, f the Coriolis parameter and ρ the water density. While winds are easterly to northeasterly year round over the Caribbean, large seasonal variations in winds are seen over the eastern Pacific warm pool. There, the northeast trades prevail converging onto the ITCZ at 5^{o}N in winter but vector winds are weak north of 10^{o}N under the ITCZ in summer. The seasonal shifts in winds are particularly large between 5-10^{o}N, from northeasterly in winter to southwesterly in summer. (The zonal band of upward Ekman pumping is generally collocated with the ITCZ that maintains positive vorticity of the surface flow.) As shown in Fig. 3, the Tehuantepec and Papagayo jets are clearly visible in summer, although considerably weaker in both speed and offshore extent than in winter. In summer, there is no evidence for climatological gap winds off Panama; instead, winds converge onto the warm continent from the ocean on both sides.

b. Effect on thermocline depth

A dipole wind-curl pattern is associated with each of the gap wind jets (Fig. 3). While the speed of the Papagayo jet decreases by half from winter to summer, surprisingly, the Ekman upwelling is strong year around. This occurs because the shear remains strong in summer between the weak Papagayo jet and the southwesterlies to the south that converge toward the Central American land bridge. As a result, the strongest annual-mean upwelling over the entire eastern Pacific warm pool is found south of the Papagayo gap rather than over the Gulf of Tehuantepec. Kessler’s (2002) calculations show that the observed thermocline topography is consistent with forcing by Ekman pumping according to linear Sverdrup dynamics. Indeed, the Ekman upwelling band southeast of the Papagayo jet axis forces a zonal band of shallow thermocline extending west along 6-12^{o}N (Fig. 4a). At the center of this Costa Rica Dome, the 20^{o}C isotherm is only 30 m deep. The 20^{o}C isotherm tracks the tightly packed thermocline quite well in this region (Fig. 5). In the zonal direction, this thermocline dome is highly asymmetric. The thermocline shoals rapidly from the Central American coast to 90^{o}W under the strong Ekman pumping associated with the Papagayo wind jet, and deepens slowly to the west where the Ekman pumping nearly vanishes. In the meridional direction, the 20^{o}C isotherm is equally shallow at the Costa Rica Dome as in the equatorial upwelling zone.

The thermocline topography and Ekman pumping are related by the following Sverdrup relation:

$$h - h_E = -\frac{f^2}{g' H\beta}\int_{x_E}^{x} w_e dx , \tag{1}$$

where h is the thermocline depth deviation from its mean value H, the subscript E denotes values at the eastern boundary, g' is the reduced gravity, β the meridional derivative of the Coriolis parameter, and x is the longitudinal coordinate. Here we have used a 1.5-layer model [Kessler (2002) discusses the limitations of such a model for the eastern tropical Pacific]. For a zonally-oriented band of Ekman upwelling like the one associated with the Papagayo jet, its effect accumulates in the zonal integral and produces a large response in the thermocline depth to the west (Fig. 4). This is the main mechanism for the generation of the Costa Rica Dome (Kessler 2002).

The orientation of a wind jet is very important for its effect on thermocline topography. In contrast to the zonally-oriented Papagayo jet, consider a meridional wind jet that is symmetric about its axis (i.e., ignore the anticyclonic inertial turning). In this case, the zonal integral in Eq. (1) sums the contributions across both sides of the meridionally oriented wind-curl dipole, so its net effect on the thermocline cancels at longitudes sufficiently far from the wind jet. Thus, the thermocline depth decrease forced by the Tehuantepec upwelling on the eastern flank of the jet is visible but highly localized, not fully developed in strength and spatial extent because of the opposing forcing by the negative vorticity on the western flank of the jet. A close inspection indicates that the Tehuantepec jet curl becomes asymmetric as it extends southward: the Ekman downwelling on the west becomes greater than the upwelling to the east (Figs. 3ab), likely an effect of Earth rotation on the jet (Clarke 1988; Steenburgh et al. 1998). This stronger downwelling of the Tehuantepec jet, helped by the downwelling of the background (especially in winter), forces a thermocline bowl centered at 107^{o}W, 13^{o}N (Fig. 4b; Kessler 2004). It is unclear what determines the orientation of a wind jet, but the geometry of the mountain pass seems to be an important factor. While the pass north of Tehuantepec favors a northerly wind jet, the Papagayo pass allows winds to accelerate only in the zonal direction, leading to a strong thermocline response that extends well to the west.

c. Effect on SST

In winter, intense cooling induced by the wind jets leaves marked signatures on the SST field. Under each of these wind jets is a band of cold water with SST well below 27^{o}C (Fig. 6b) due to increased surface heat flux and vertical mixing. This wind-induced cooling is so strong that the minimum SST is less than 25^{o}C in this multi-season average map, against background SSTs of 28^{o}C or above in the warm pool. The SST minima are roughly aligned with the axes of wind jets, and the cooling trails the mountain passes over a long distance. The thermocline topography appears to also be an important factor for surface cooling, and although a quantitative heat balance is beyond the scope of this paper, some conclusions about the importance of surface heat fluxes versus stirring from the shallow thermocline can be drawn. Note that the Papagayo cooling is roughly collocated with the thermocline ridge and extends 1000 km offshore while the Tehuantepec cooling extends only half as far because its upwelled thermocline is confined closer to the coast (Fig. 4b). Also, the coldest SST appears to be found slightly offshore (Fig. 4), as the thermocline shoals (Fig. 5a), not precisely under the strongest winds at the coast. The strong entrainment made possible by strong winds and a shallow thermocline is further manifested in a tongue of high chlorophyll concentrations as observed by the SeaWiFS satellite over each of the Tehuantepec, Papagayo and Panama jets (Fig. 6b). In winter, the shallow thermocline in the Costa Rica Dome and off the coast of South America, which is itself a response to the vorticity forcing by the Papagayo and Panama jets, aids the wind-induced cooling. The maximum cooling and the thermocline depth minimum are roughly collocated over these two cold patches, allowing them to extend far offshore.

While the cold patches in the annual mean SST map are dominated by the winter cooling, there are interesting features in summer SST. The summer SST distribution in the warm pool is very different from that in winter (Fig. 8). SST contours are zonally oriented south of 10^{o}N and become somewhat parallel to the coast near Central America. A weak cold wedge develops offshore of the Gulfs of Tehuantepec and Papagayo. The cooling over the Gulf of Tehuantepec seems a weaker echo of its stronger counterpart in winter, but the cooling off Papagayo extends much farther offshore than the wind jet (Fig 3c), suggesting the importance of the shallow thermocline and resulting entrainment, rather than the effect of surface heat flux, for the open-ocean cooling in summer. At and south of 10^{o}N, summer cooling is located at the top of the Costa Rica Dome (Fig 4c), where the ocean mixed layer is only about 10 m deep (Fig. 5) and the 20^{o}C isotherm is shallower than 30m. The doming thermocline there allows cold water to be upwelled or easily entrained into the mixed layer. Further west, the thermocline deepens and summer SST can warm (Figs. 4c and 7), However, high chlorophyll activity in summer is organized into a zonal patch centered at 9^{o}N extending 10^{o} in longitude and 5^{o} in latitude, closely collocated with the 40 m depth contour of the 20^{o}C isotherm (Fig. 7). The difference between the patterns of SST and chlorophyll suggests that the high chlorophyll in the western Costa Rica Dome is due to biological activity below the surface mixed layer, which is shallow enough to receive sufficient sun light for photosynthesis, but too deep to easily entrain cool water to the surface. In-situ observations are necessary to test this hypothesis.

d. SST feedback on atmosphere

With the wind jets strongest and the SST features most sharply defined in winter (Fig. 6a), one might expect that their effects on atmospheric convection through the cold SST patches would also be strongest in winter. This is true for the Panama jet; the cold patch it induced suppresses atmospheric convection, giving rise to a band of local minimum in precipitation (Fig. 8b). However, the Tehuantepec and Papagayo jets and associated cold patches have little effect on winter precipitation because they are located in a dry region north of the ITCZ. West of about 110°W, the winter ITCZ is roughly collocated with the high SST band, but further east it is kept south of 7°N and consistently displaced to the southern boundary of the eastern Pacific warm pool[1] (Fig. 8b).

In boreal summer, the ITCZ takes a more northerly position, occupying a large latitudinal band between 7°N and 15°N that covers the cold patch over the Costa Rica Dome (Fig. 8c). Within this broad ITCZ, there is a hole of precipitation deficit over the cold spot on top of the Costa Rica Dome. This hole in the ITCZ is over 500 km in diameter with a 50% drop in precipitation (5 mm/day in the hole vs. 10 mm/day on the background). Below the dry hole, SST reaches a minimum in the zonal direction, suggesting that the cold spot forces the rainfall deficit. If we assume that cloudiness is roughly proportional to precipitation in this region of deep convection, the increased solar radiation under the dry hole is a negative feedback that acts to dampen the cold spot in SST, further supporting the notion that the thermocline dome maintains both the cold spot and hole in the ITCZ.

The weak summer jet off Tehuantepec leaves small but visible signatures in both SST and chlorophyll, but apparently not in precipitation. Probably this is because the SST remains above 28.5°C under the summer jet (Fig. 8b). Neither the Tehuantepec nor Panama jets have much effect on the thermocline depth in summer. The Costa Rica Dome, by contrast, is strong year around. This permanent thermocline dome is a result of upwelling curl associated in winter with the Papagayo jet, helped by its orientation that efficiently excites the thermocline response, and in summer, additionally by the positive curl of the

[1] In winter, as the prevailing easterly trades impinge on the Central American mountains, orographic downdraft suppresses convection off the Pacific coast, displacing the ITCZ away from the bulk of the warm pool. Numerical experiments using the model described in the Appendix indicate that this effect of the broad mountain range conceals the effect of shorter-scale gap winds on convection off Tehuantepec and Papagayo in winter (not shown).

ITCZ. As a result, SST over the Costa Rica Dome remains below 28.5°C throughout the seasonal cycle (Fig. 8), which inhibits atmospheric convection when the ITCZ moves overhead in summer. Although the winter Papagayo jet does not have a direct effect on winter atmospheric convection, its curl makes an important contribution to maintaining the robust thermocline dome that persists throughout the year. If not for the winter jet, the Ekman upwelling would be only a result of the ITCZ, and thus would be in phase with the precipitation, as it is west of 90°W (Fig. 12a and c); cool SST due to entrainment would lag precipitation by 90° and have only a small, delayed effect. Thus, the cold spot and the collocated rainfall deficit in summer may be viewed as partly resulting from the winter forcing through the ocean memory in the form of the Costa Rica Dome.

In September, the climatological Papagayo jet disappears altogether, with winds directed onshore instead of offshore (Figs. 9a, and 12a show that the onshore winds last only about one month). The curl, however, remains weakly positive (Fig. 12a). Thus the September climatology offers an example showing that the direct wind forcing of the weak summer Papagayo jet is not essential for the cold spot and resulting dry hole in the ITCZ. Thus, the effect must be due to the persistent shallow thermocline of the Costa Rica Dome. Indeed, the cold SST spot around 90^{o}W remains of the same strength as the summer mean and reaches all the way to the coast of Central America, causing a precipitation reduction in a 5^{o}x5^{o} area.

The dry hole in the summer ITCZ is not visible in the popular 2.5^{o}x2.5^{o} CMAP rainfall product, probably because of insufficient resolution and spatial smoothing. Its existence is confirmed by higher-resolution datasets based on independent rainfall measurements by the TRMM PR and infrared (IR) instruments on the TRMM and geostationary satellites (Fig.

10). While noisy, the PR observations show increased rainfall on the coast, ruling out the possibility of direct orographic origin of this dry hole. Degraded in spatial resolution but with excellent sampling, IR measurements reaffirm that this hole of rainfall deficit is found offshore roughly collocated with the Costa Rica Dome.

To test the effect of orography, we carried out a high-resolution simulation with a regional atmospheric model briefly described in the Appendix. Figure 11 shows the simulated rainfall for August 1999. While the simulated ITCZ is too thick in its meridional width west of 105^{o}W, the model captures the salient features of the observed summer rainfall pattern. In particular, pronounced rainfall deficits are found over the open ocean near the Costa Rica Dome. This hole of rainfall deficit remains in an additional experiment in which the land orography on Central American is removed and set uniformly at 0.5 m above the sea level.

The ITCZ is twice as strong in summer as in winter in terms of precipitation over the eastern Pacific (note the difference in color scale between Figs. 8ab and 8c). As a result, the annual-mean rainfall distribution bears a strong resemblance to the summer distribution (Fig. 8a). The annual-mean ITCZ is broad west of 95^{o}W, occupying a latitudinal band of 5-13^{o}N. East of 95^{o}W, it narrows with the axis trending south into the Gulf of Panama (Fig 8a). The summer Costa Rica Dome effect leaves a clear mark in the annual-mean field that appears as a region of minimum rainfall off Papagayo. In contrast to the strong summer effect on annual-mean rainfall, the annual-mean SST resembles the winter field featuring all three cool patches off Tehuantepec, Papagayo and Panama.

e. Seasonal cycle

Having discussed seasonal mean climate in summer and winter, we now describe the full seasonal cycle along 10°N (Fig. 12), a latitude that cuts through the Costa Rica Dome. SSH and thermocline depth are related by SSH=g'h/g in a 1.5-layer model, and we will use terms of SSH and thermocline depth interchangeably here. We use SSH to describe thermocline depth variations because it is better sampled with satellite observations. The 20°C isotherm shows a similar seasonal cycle, albeit smoother in space and time (not shown).

The positive curls off Papagayo are strong nearly year around and are responsible for the permanent thermocline dome to the west. The gap winds vanish in September and October (Fig. 12a) when the Atlantic ITCZ takes its northernmost position, relaxing the pressure gradient across Central America. The seasonal cycle in thermocline depth behaves differently east and west of 90°W, which is where SSH variance is at its zonal minimum. East of 90°W, the strong wind jet and its curl force the thermocline to shoal in winter; then the near-shore thermocline deepens in summer as the gap winds weaken. Wind curls display a seasonal cycle of an opposite phase west of 90°W, negative in winter when the ITCZ is to the south and positive in summer when the ITCZ is overhead. The latent heat release by ITCZ convection generates positive vorticity in the lower troposphere, which in turn forces an Ekman suction that lifts the thermocline. While the Ekman pumping variation is more or less stationary in space, the thermocline response displays a clear westward propagation indicative of Rossby waves (Fig. 12b). West of 90°W, the thermocline deepens during the first half of the year and shoals during the second half. Because of the opposite phasing in Ekman pumping variations to its east and west, the center of the Costa Rica Dome at 90°W experience little seasonal variations. A 1.5-layer linear reduced-gravity model simulates this observed annual cycle in SSH rather well (not shown), suggesting that these simple wave dynamics dominate the seasonal timescale (Kessler 2004).

In winter, the cold patch induced directly by the strong Papagayo jet cuts through 10^{o}N at 88^{o}W. This cold patch starts to develop in October, reaches a maximum in February, and persists through April (Fig. 12c). In May, the summer regime begins to take over, with SST reaching its seasonal maximum and the ITCZ covering this latitude, but SST over the dome is still cooler than either to the east or west (Fig. 12c). During the summer, there is a weak but persistent minimum in SST around 90^{o}W, the center of the Costa Rica Dome. A region of reduced rainfall is roughly collocated with the region of SST minimum during May-October. The rainfall deficit over the Costa Rica Dome is especially large in July and August, with values less than half of that at 100^{o}W.

The seasonal variations in chlorophyll are quite complicated but generally follow the thermocline depth variations with a lag of 0-2 months (Fig. 12b). At the center of the Costa Rica Dome (90^{o}W) SeaWiFS chlorophyll reaches a seasonal maximum in May when SSH reaches a minimum. Further to the west, chlorophyll reaches a seasonal minimum during May-June two months after the SSH maximum. SSH's control over chlorophyll variations is further corroborated by their westward co-propagation. The seasonal cycle of chlorophyll seems to be induced not by the local Ekman pumping—the two are roughly in quadrature in phase west of 95^{o}W. Instead, the chlorophyll cycle is consistent with an equilibrium response to thermocline depth.

4. Summary

We have used a suite of new satellite observations to study air-sea interaction over the eastern Pacific warm pool. The use of these satellite observations allows us to map the co-varying ocean-atmospheric structure in detail never possible before. Our analysis not only confirms the existence of strong atmospheric dynamic and thermodynamic forcing of the ocean in winter but also reveals that patterns of SST induced by ocean dynamics force the atmosphere on short spatial scales in boreal summer. In winter as the pressure difference between the tropical northwestern Atlantic and northeastern Pacific builds up, the mountains of Central America funnel strong winds through three major passes: Tehuantepec, Papagayo and Panama. The Papagayo pass, in particular, directs a westward wind jet over the Pacific. The positive wind stress curl south of this wind jet is strongest in winter but exists almost year round, forcing a thermocline dome centered about 200 km offshore (the Costa Rica Dome). The thermocline depth at the center of this dome is shallow all year, with an ocean mixed layer only about 10 m deep. This thermocline dome allows cold water to be easily mixed into the mixed layer, giving rise to a cold spot in summer SST and a collocated patch of high chlorophyll activity. This surface cooling at the top of the Costa Rica Dome suppresses atmospheric convection, opening a large hole of reduced rainfall in the ITCZ southwest of Papagayo.

The Tehuantepec, Papagayo and Panama wind jets and their cooling effect on the winter SST are a well-known phenomenon. Although all three jets have pronounced (3°C) effects on winter SST, we have shown that the effect on precipitation is different among the three jets, depending on their latitude with respect to the ITCZ and its annual march, the orientation of the jets, and their correlation with upwelling curl in the ITCZ itself. The

Panama jet produces a gap in the winter ITCZ, which is at its southernmost position when the jet is strong. The Tehuantepec jet has little effect on ITCZ precipitation at any time of year because it is far to the north of the ITCZ when the jet is strong in winter, and its summer SST signature is small. The Papagayo jet makes a hole in the ITCZ in summer, because persistent upwelling curl, combined with Rossby wave radiation from the strong zonally-oriented winter jet, shoals the thermocline throughout the year and maintains cool SST even in summer.

Thermocline domes are observed in other parts of the world ocean, and their importance for marine biology is well known because of their supply of nutrients. The climatic effect of these domes has just begun to be recognized. Over these domes, cold thermocline water can easily come into contact with the sea surface either by Ekman pumping or by turbulent mixing. As a result, the thermocline depth and its variations exert a strong influence in SST over these domes. In the South Indian Ocean dome, for example, interannual Rossby waves modulate the thermocline dome at 5-10^{o}S, producing strong variations in SST, atmospheric convection, and tropical cyclones (Xie et al. 2002; Yamagata et al. 2004; Annamalai and Murtugudde 2004). The present study of the Costa Rica Dome reaffirms enhanced air-sea interaction over thermocline domes. The eastern Pacific warm pool is also an important region for cyclogenesis (e.g., Maloney and Hartmann 2000), so the surface cooling due to the Costa Rica Dome may affect the formation of eastern Pacific hurricanes.

Mountains perturb airflow and commonly leave distinct marks on surface winds over coastal waters or near islands (Chelton et al. 2004). If mountains are so configured that orographical-induced wind-curl patches are nearly zonally oriented, ocean Rossby waves are optimally excited. Because the ocean adjustment is slow and subject to weak dissipation, orographical-triggered air-sea interaction may have long lasting effects in both the ocean and atmosphere. The Costa Rica Dome and its effect on summer convection revealed in this study, and the long wake of the Hawaiian Islands in various ocean-atmospheric fields (Xie et al. 2001) are such examples. The full extent of orographical-triggered air-sea interaction has just begun to be unraveled by satellite observations which have brought unprecedented spatial resolution and temporal coverage. With increasing computing power, global models will eventually reach sufficient resolutions to resolve orographic features such as the mountain ranges of Hawaii and Central America. When they do, orographic-induced air-sea coupled phenomena documented here and elsewhere will serve as a benchmark for these models to reproduce. Toward this direction, a high-resolution coupled ocean-atmosphere model run on Japan's Earth Simulator is producing encouraging results showing signs of the ocean-atmosphere wake of Hawaii and the Costa Rica Dome (A. Sumi and T. Sakamoto, 2003, personal communication).

Acknowledgments. This study was initiated during the first author's visit to Hokkaido University, Japan. He wishes to thank Y. Tanimoto, H. Tokinaga, faculty and students at Division of Ocean and Atmospheric Science for their hospitality, and J. Hafner for data processing. TMI and QuikSCAT products are obtained from Remote Sensing Systems, chlorophyll from Goddard DAAC, TRMM 3A25G2 and 3B43 products from EORC/JAXA, Japan, and SSH from the Collecte Localisation Satellites, France. Supported by NASA, NOAA, NSF, Japan Society for the Promotion of Science, and Frontier Research System for

Global Change. IPRC publication #xxx, SOEST publication #yyy, and PMEL publication #2677.

APPENDIX

Atmospheric Model

A regional atmospheric model developed at the International Pacific Research Center of University of Hawaii is used. It is a primitive equation model solved on a longitude-latitude grid with sigma as the vertical coordinate. Its comprehensive physical package includes an E-ε closure scheme for turbulence, cloud microphysics for grid-scale clouds and precipitation, a mass-flux cumulus parameterization for subgrid-scale convection, a cloud-interactive radiation scheme, and a land surface model. See Wang et al. (2004) and Xu et al. (2004) for a detailed description of the model and its performance over the eastern Pacific.

Here the model resolution is set at 0.25° in horizontal and 28 levels in the vertical. The initial and lateral boundary conditions are constructed based on the National Centers for Environmental Prediction/National Center for Atmospheric Research (NCEP/NCAR) reanalysis (Kalnay et al. 1996). The lateral boundary conditions are updated four times daily. The surface boundary conditions are the weekly $1^{\circ}\times1^{\circ}$ Reynolds and Smith SST product. The model domain covers a region of 125°W-75°W, 10°S-27.5°N. Land topography is based on the USGS ETOPO dataset. The model is initialized on June 25, 1999 and integrated for three months.

REFERENCES

Annamalai, H., and R. Murtugudde, 2004: Role of the Indian Ocean in regional climate variability. In *Ocean-Atmosphere Interaction and Climate Variability*, C. Wang et al. (eds.), Geophys. Monograph, Amer. Geophys. Union, in press.

Barton, W.D., M.L. Argote, J. Brown, P.M. Kosro, M. Levin, J.M. Robles, R.L. Smith, A. Trasvina, and H.S. Velez, 1993: Supersquirt: Dynamics of the Gulf of Tehuantepec, Mexico. *Oceanogr*., **6**, 23-30.

Chelton, D.B., M.H. Freilich, and S.N. Esbensen, 2000: Satellite observations of the wind jets off the Pacific coast of Central America. Part I: Case studies and statistical characteristics. *Mon. Wea. Rev*., **128**, 1993-2018.

___, M.G. Schlax, M.H. Freilich, and R.F. Milliff, 2004: Satellite measurements reveal persistent small-scale features in ocean winds. *Science*, **303**, 978-983.

Chiang, J.C.H., Y. Kushnir, and S.E. Zebiak, 2000: Interdecadal changes in eastern Pacific ITCZ variability and its influence on the Atlantic ITCZ. *Geophy. Res. Lett*., **27**, 3687-3690.

Clarke, A.J., 1988: Inertial wind path and sea surface temperature patterns near the Gulf of Tehuantepec and the Gulf of Papagayo. *J. Geophys. Res*., **93**, 15 491-15 501.

Ducet, N., P. Y. Le Traon, and G. Reverdin, 2000: Global high-resolution mapping of ocean circulation from TOPEX/Poseidon and ERS-1 and –2. *J. Geophys. Res*., **105**, 19 477-19 498.

Fiedler, P.C., 2002: The annual cycle and biological effects of the Costa Rica Dome. *Deep-Sea Res. I*, **49**, 321-338.

Hofmann, E.E., A.J. Busalacchi, and J.J. O'Brien, 1981: Wind generation of the Costa Rica Dome. *Science*, **214**, 552-554.

Kalnay, E., and Coauthors, 1996: The NCEP/NCAR 40-year re-analysis project, *Bull. Amer. Meteor. Soc.*, **77**, 437-471.

Legeckis, R., 1988: Upwelling off the Gulfs of Panama and Papagayo in the tropical Pacific during March 1985. *J. Geophys. Res.*, **93**, 15 485-15 489.

Liu, W.T., X. Xie, P.S. Polito, S.-P. Xie and H. Hashizume, 2000: Atmospheric manifestation of tropical instability waves observed by QuikSCAT and Tropical Rain Measuring Mission. *Geophys. Res. Lett.*, **27**, 2545-2548.

Kessler, W.S., 2002: Mean three-dimensional circulation in the Northeast tropical Pacific. *J. Phys. Oceanogr.*, **32**, 2457-2471.

___, 2004: The circulation of the eastern tropical Pacific: A review. *Progress in Oceanography*, Pergamon, submitted.

Maloney, E.D., and D.L. Hartmann, 2000: Modulation of eastern North Pacific hurricanes by the Madden-Julian Oscillation. *J. Climate*, **13**, 1451-1460.

McCreary, J.P., H.S. Lee, and D.B. Enfield, 1989: Response of the coastal ocean to strong offshore winds: With application to circulations in the Gulf of Tehuantepec and Papagayo. *J. Mar. Res.*, **47**, 81-109.

___, P. Lu, and Z. Yu, 2002: Dynamics of the Pacific subsurface countercurrents. *J. Phys. Oceanogr.*, **32**, 2379-2404.

Mitchell, T.P. and J.M. Wallace, 1992: The annual cycle in equatorial convection and sea surface temperature. *J. Climate*, **5**, 1140-1156.

Reynolds, R.W., and T.M. Smith, 1994: Improved global sea surface temperature analyses using optimal interpolation, *J. Climate*, **7**, 929-948.

Schultz, D.M., W.E. Bracken, L.F. Bosart, G.J. Hakim, M.A. Bedrick, M.J. Dickinson, and K.R. Tyle, 1997: The 1993 Superstorm cold surge: Frontal structure, gap flow and tropical impact. *Mon. Wea. Rev*., **125**, 5-39.

Steenburgh, W.J., D.M. Schultz, and B.A. Colle, 1998: The structure and evolution of gap outflow over the Gulf of Tehuantepec, Mexico. *Mon. Wea. Rev*., **126**, 2673-2691.

Umatani, S., and T. Yamagata, 1991: Response of the eastern tropical Pacific to meridional migration of the ITCZ: The generation of the Costa Rica Dome. *J. Phys. Oceanogr*., **21**, 346-363.

Wang, C., and D.B. Enfield, 2003: A further study of the tropical Western Hemisphere warm pool. *J. Climate*, **16**, 1476-1493

Wang, Y., S.-P. Xie, H. Xu, and B. Wang, 2004: Regional model simulations of marine boundary layer clouds over the Southeast Pacific off South America. Part I: Control experiment. *Mon. Wea. Rev*., **132**, 274-296.

Wentz, F. J., C. Gentemann, D. Smith, and D. Chelton, 2000: Satellite measurements of sea surface temperature through clouds. *Science*, **288**, 847-850.

Wyrtki, K., 1964: Upwelling in the Costa Rica Dome. *Fish. Bull*., **63**, 355-372.

Xie, P., and P. A. Arkin, 1996: Analyses of global monthly precipitation using gauge observations, satellite estimates, and numerical model predictions. *J. Climate*, **9**, 840–858.

Xie, S.-P., 2004a: The shape of continents, air-sea interaction, and the rising branch of the Hadley circulation. In *The Hadley Circulation: Past, Present and Future*, H. F. Diaz and R. S. Bradley (eds.), Kluwer Academic Publishers, Dordrecht, in press.

___, 2004b: Satellite observations of cool ocean-atmosphere interaction. *Bull. Amer. Meteor. Soc.*, **85**, 195-208.

___, H. Annamalai, F.A. Schott and J.P. McCreary, 2002: Structure and mechanisms of South Indian Ocean climate variability. *J. Climate*, **15**, 864-878.

___, W.T. Liu, Q. Liu and M. Nonaka, 2001: Far-reaching effects of the Hawaiian Islands on the Pacific Ocean-atmosphere. *Science*, **292**, 2057-2060.

Xu, H., Y. Wang and S.-P. Xie, 2004: Effects of the Andes on eastern Pacific climate: A regional atmospheric model study. *J. Climate*, **17**, 589-602.

Yamagata, T., S. K. Behera, J. J. Luo, S. Masson, M. R. Jury, and S. A. Rao, 2004: Coupled ocean-atmosphere variability in the tropical Indian Ocean. In *Ocean-Atmosphere Interaction and Climate Variability*, C. Wang et al. (eds.), Geophys. Monograph, Amer. Geophys. Union, in press.

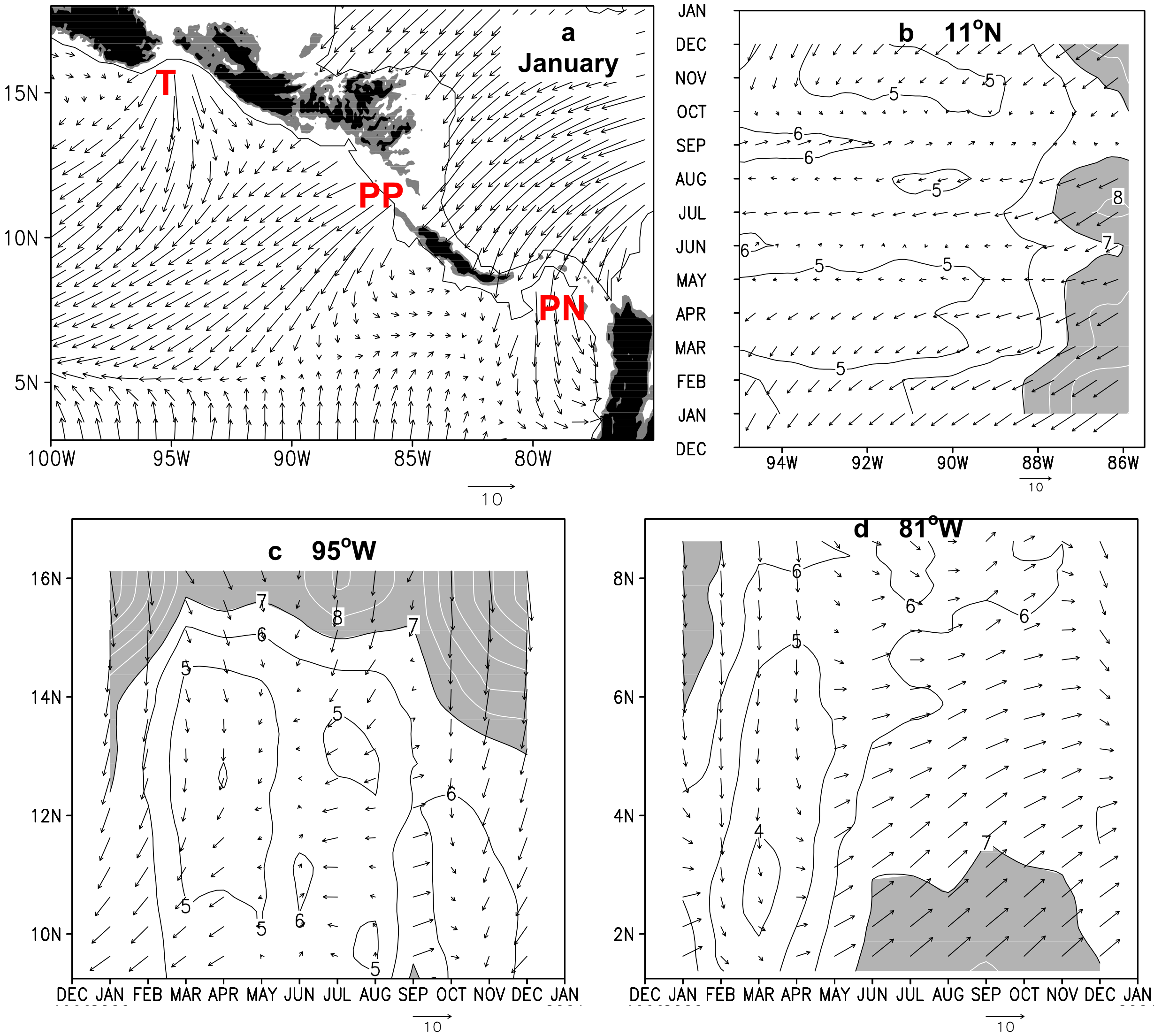

Fig. 1. a) Wind jets over the Gulfs of Tehuantepec (T), Papagayo (PP), and Panama (PN) in the QuikSCAT surface wind velocity (m/s) climatology for January. b) Longitude-time section of wind velocity (u, v) and scalar speed (contours; shade > 7m/s) at 11^{o}N (Papagayo gap). Latitude-time sections of wind velocity and scalar speed (contours; shade > 7m/s): c) at 81^{o}W (Panama gap), and d) at 95^{o}W (Tehuantepec gap). In (a), the light and dark shades denote topography greater than 500 and 1000 m, respectively.

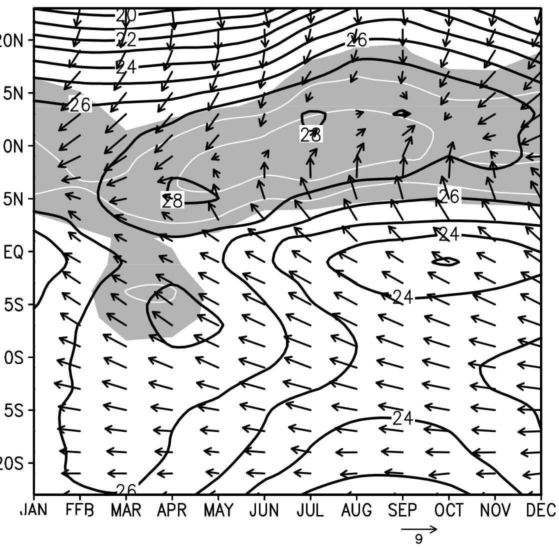

Fig. 2. Time-latitude section of climatological SST (black contours in in ^{o}C), surface wind vectors (m/s), based on COADS; and CAMP precipitation (white contours at 5 mm/day intervals; shade > 2.5 mm/day). All zonally averaged in 120-115^{o}W.

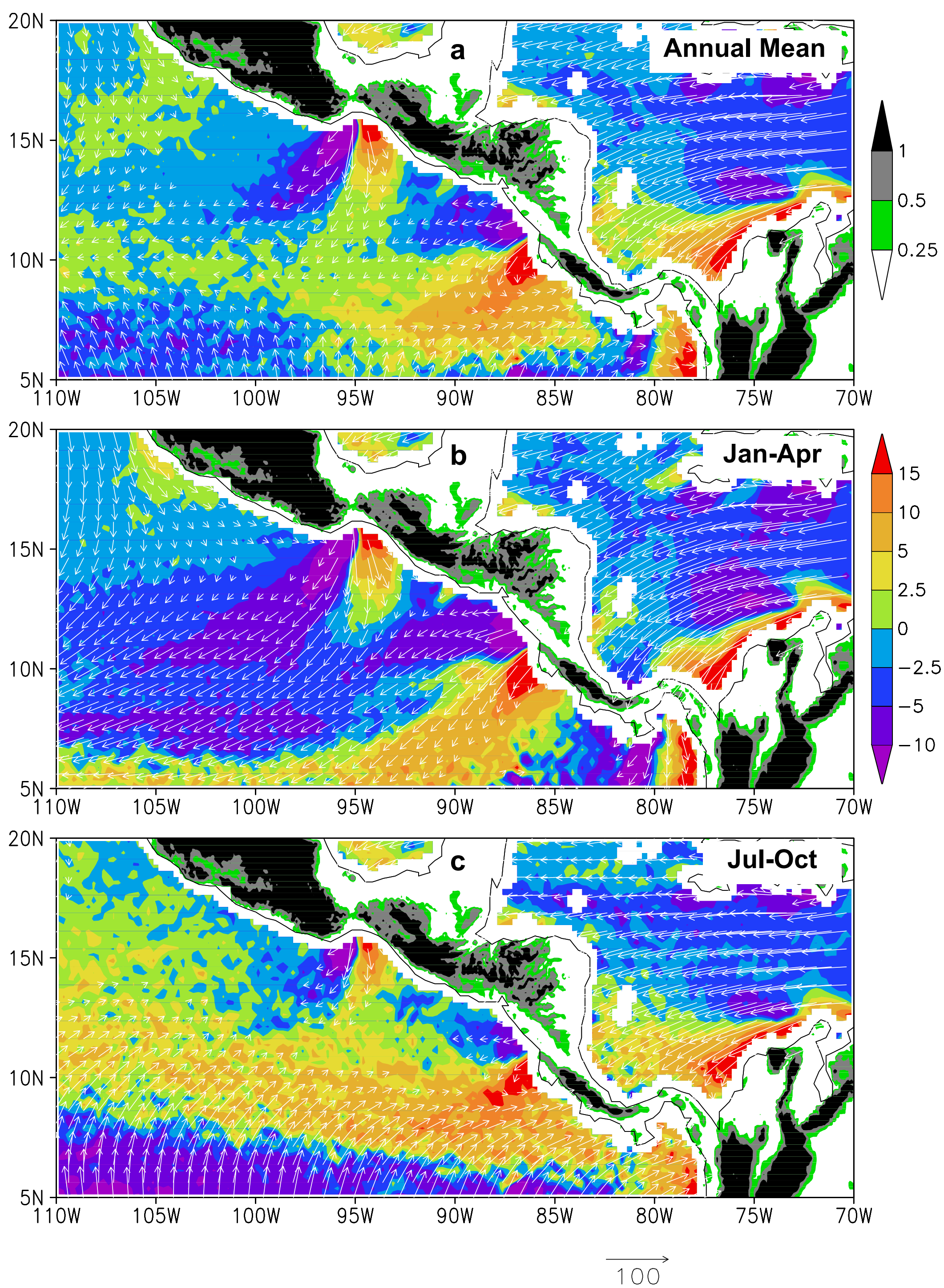

Fig. 3. QuikSCAT pseudo wind stress (vectors in m^2s^{-2}) and Ekman pumping velocity (shade in 10^{-6} m/s) climatology. (a) Annual mean, (b) January-April, and (c) July-October. Land orography (km) is plotted in color shading.

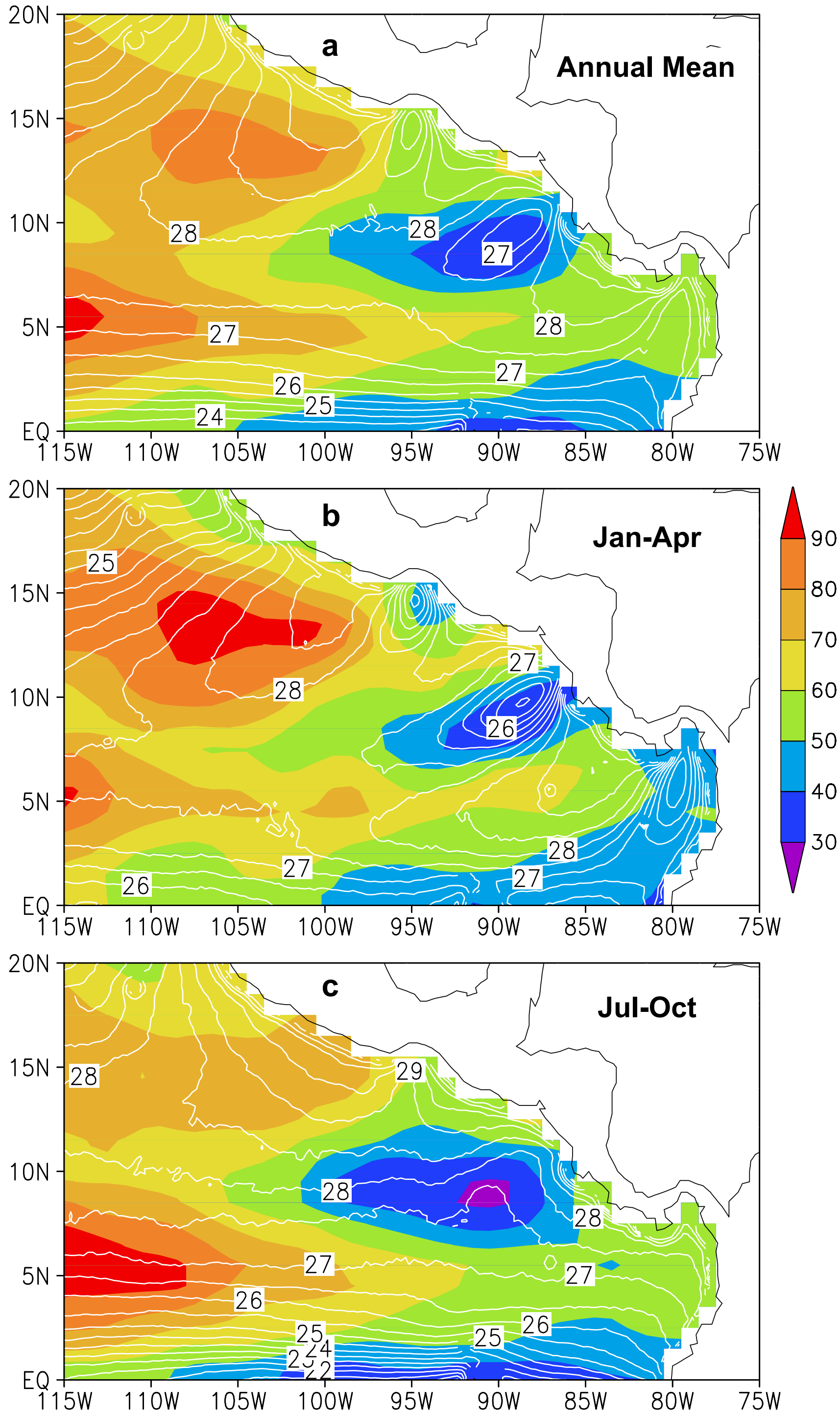

Fig. 4. Climatology of SST (contours at internals of 0.5°C) and the 20°C isotherm depth (color in m). (a) Annual mean, (b) January-April, and (c) July-October.

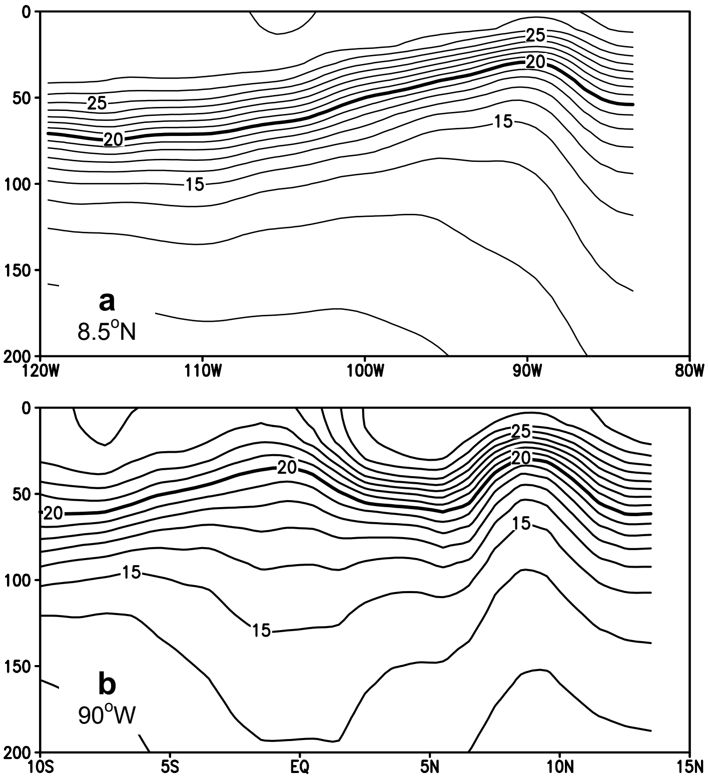

Fig. 5. Mean ocean temperature (^{o}C) along (a) $8.5^{o}N$ and (b) $90^{o}W$.

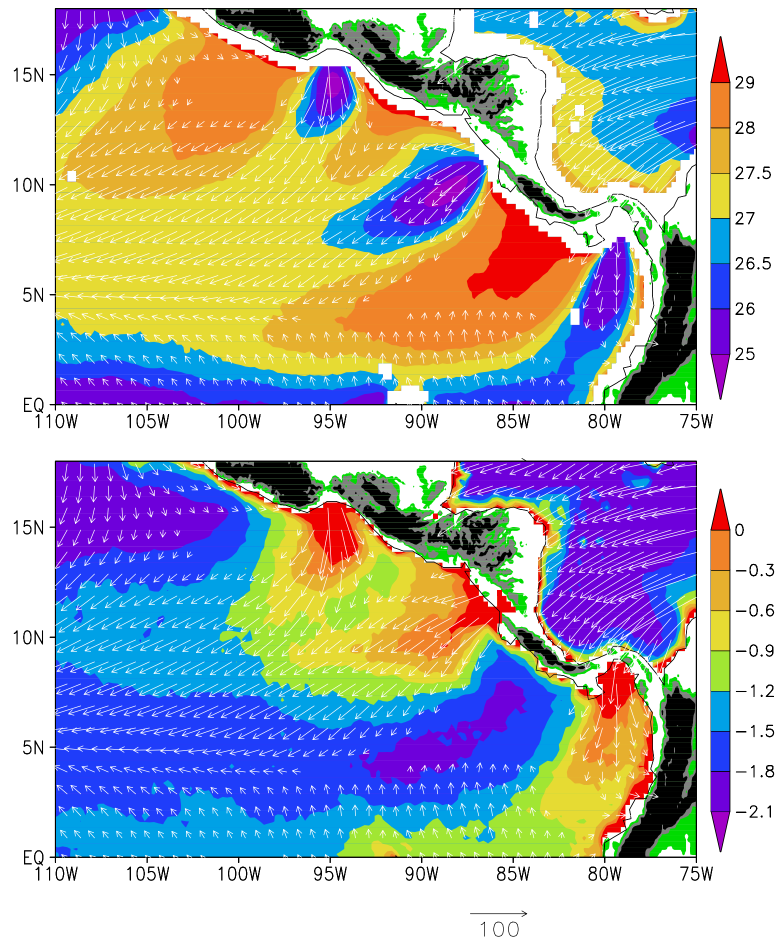

Fig. 6. January-March climatology: QuikSCAT pseudo wind stress (vectors in m^2s^{-2}), TMI SST (top panel in ^oC) and SeaWiFS chlorophyll in natural logarithm (bottom in mg/m^3).

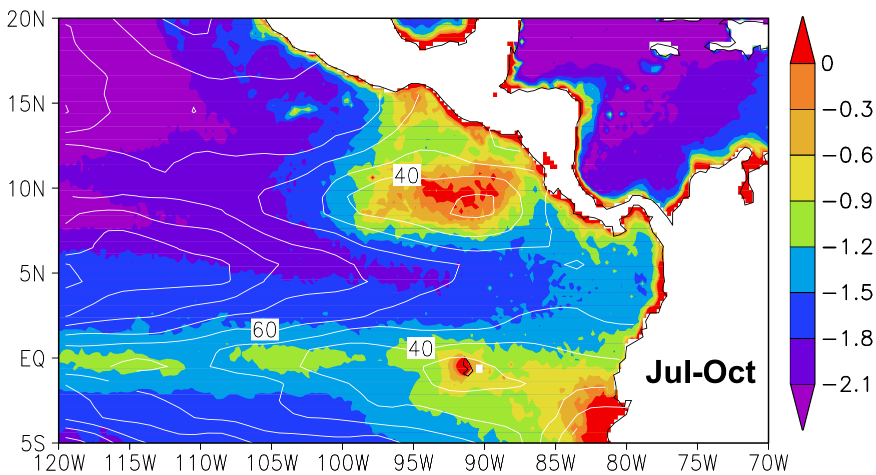

Fig. 7. SeaWiFS chlorophyll in natural logarithm (shade in mg/m^3) and 20^oC isothermal depth (contours in m) climatology for July-October.

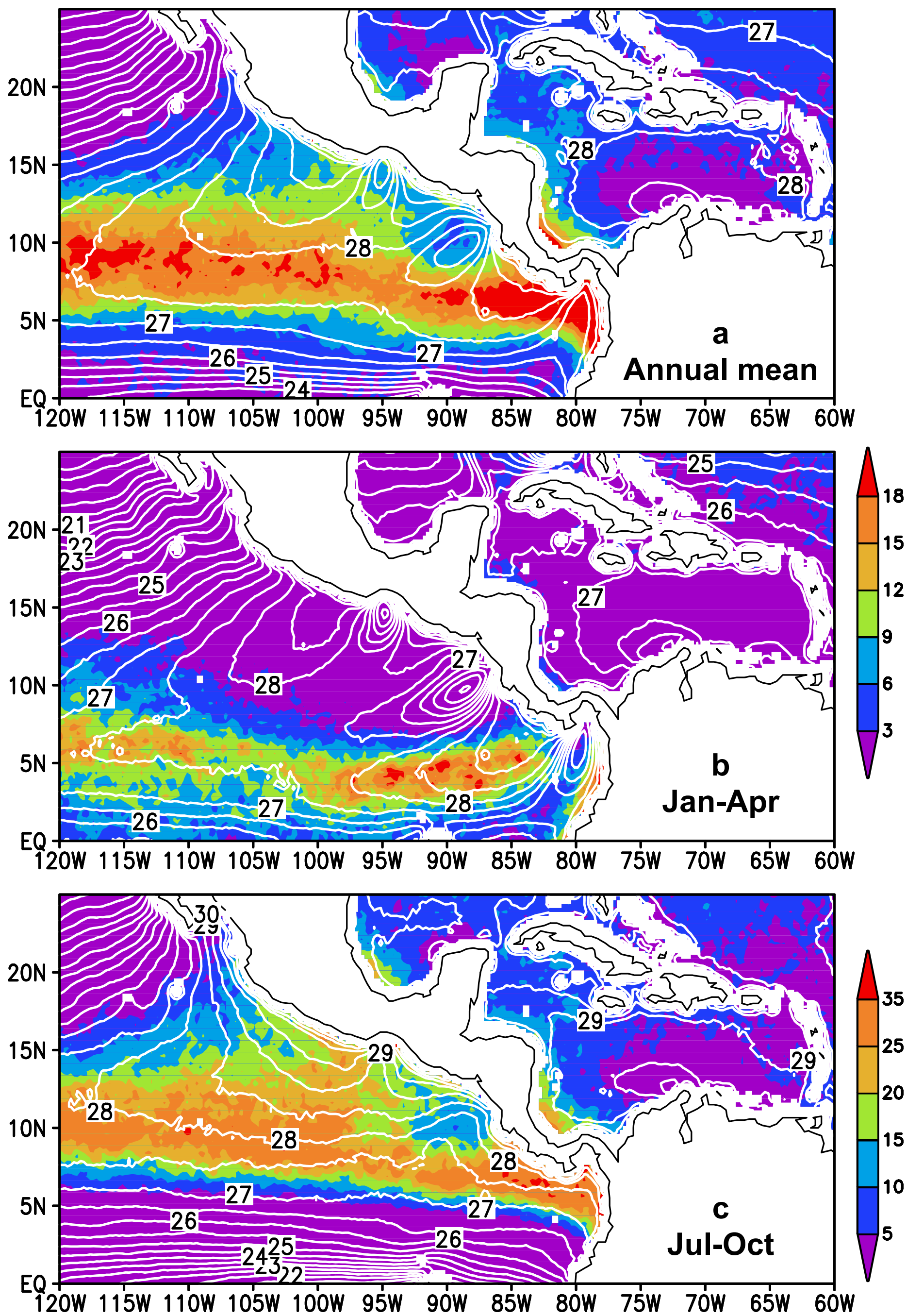

Fig. 8. TMI SST (contours in °C) and precipitation (shade in mm/day) climatology. (a) Annual mean, (b) January-April, and (c) July-October. Note the different color scale for the lower panel for summer.

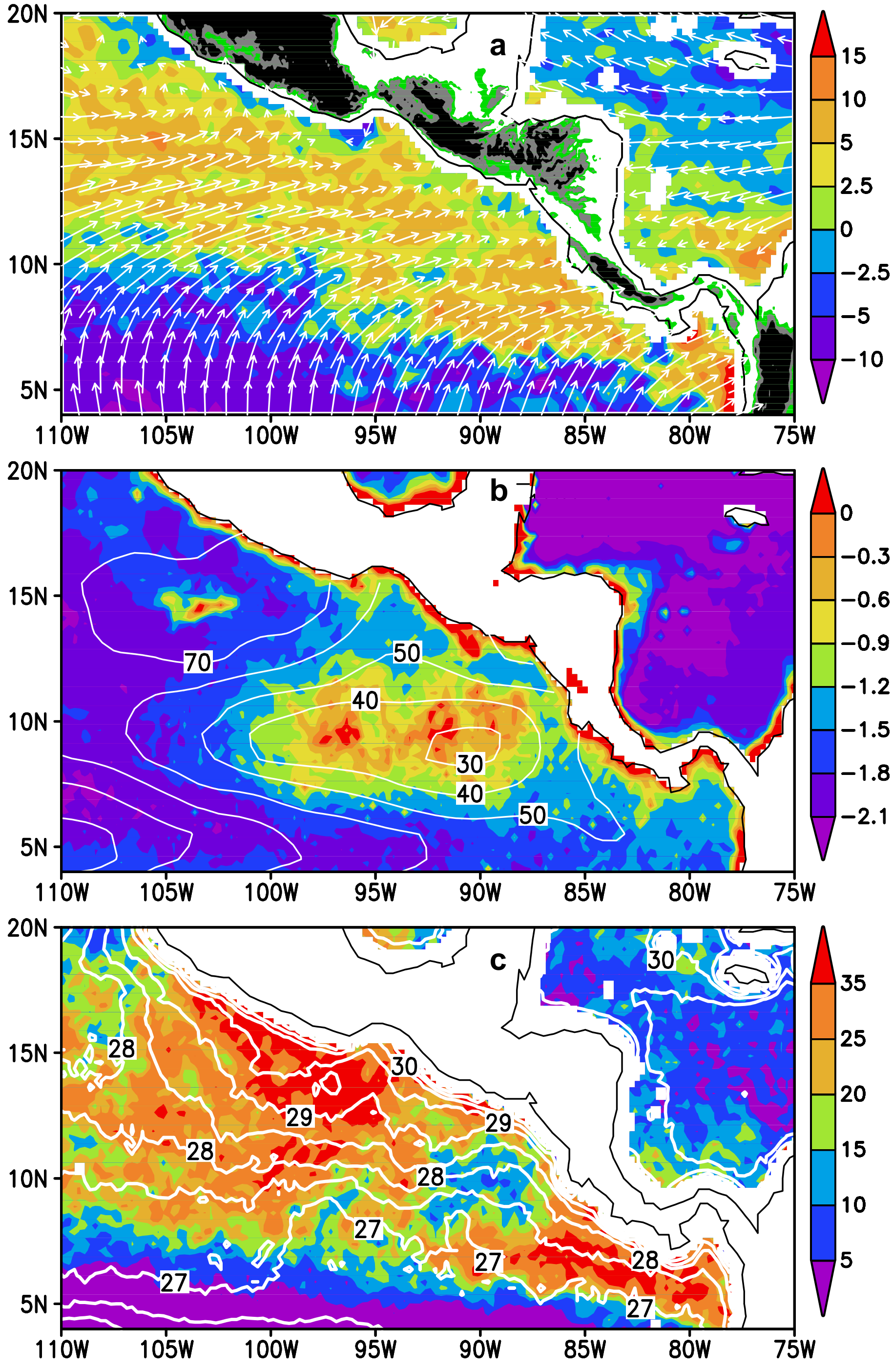

Fig. 9. September Climatology. (a) QuikSCAT pseudo wind stress (vectors in m^2s^{-2}) and Ekman pumping velocity (color in 10^{-6} m/s); (b) SeaWiFS chlorophyll in natural logarithm (color in mg/m^3) and 20^{o}C isothermal depth (contours in m); (c) TMI precipitation (color in mm/day) and SST (contours in ^{o}C).

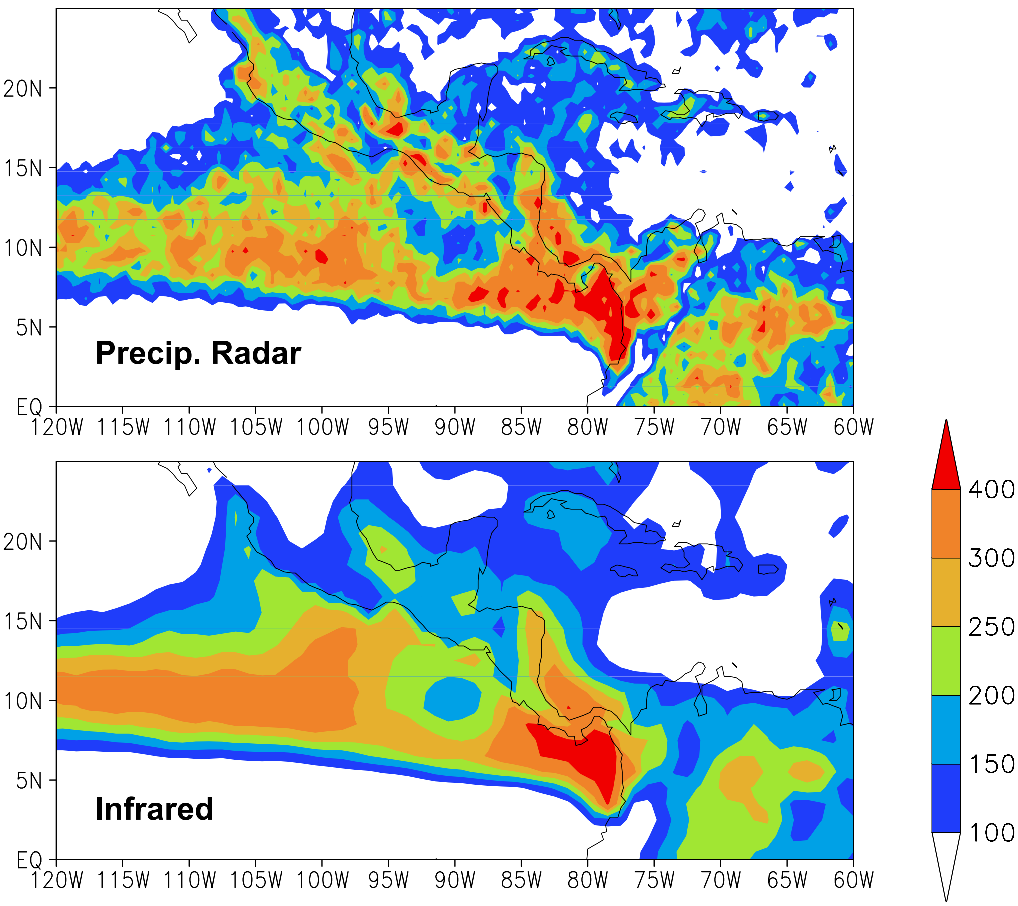

Fig. 10. July-October precipitation (mm/month) based on the TRMM PR (3A25G2) and infrared (3B43) measurements.

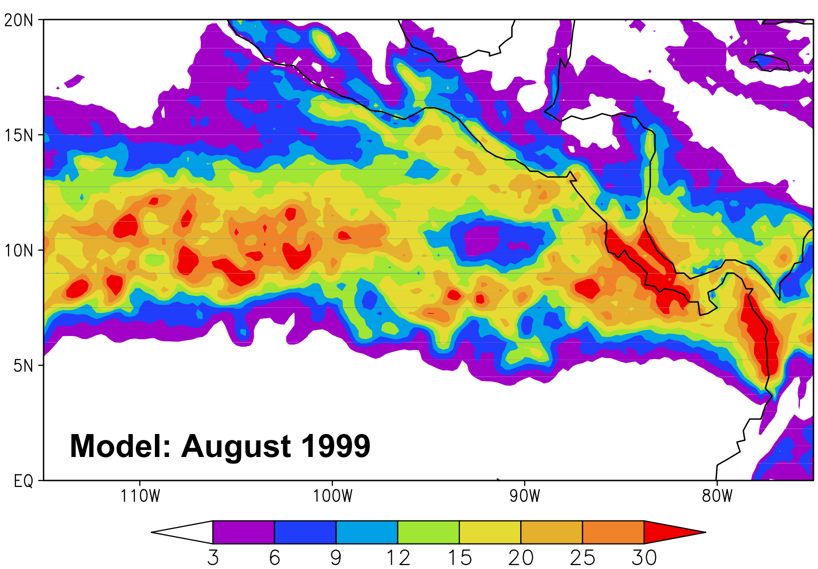

Fig. 11. Precipitation (mm/day) in a regional atmospheric model, averaged for August 1999.

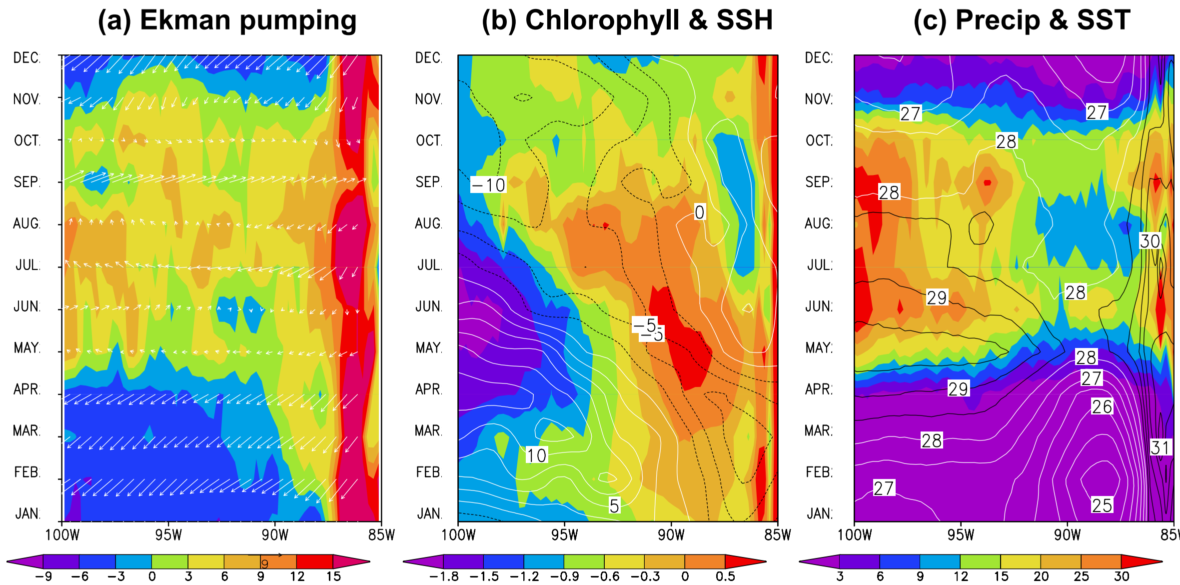

Fig. 12. Longitude-time sections averaged in 9-11^{o}N: from left, wind velocity (m/s) and Ekman pumping velocity (shade in 10^{-6} m/s); Chlorophyll in natural logarithm (color in mg/m^3) and merged sea level height (contours in cm); TMI precipitation (shade in mm/day) and SST (contours in ^{o}C).